RSC Advances

PAPER

View Article Online
View Journal | View Issue

Cite this: *RSC Adv.*, 2025, **15**, 4681

Removal of methyl orange and methylene blue by bimetallic zinc/cobalt metal–organic skeleton/carbon nanotubes (Zn/Co-ZIF@CNTs)

Guofu Huang,†[a] Yijie Zhang,†[b] Ranran Zhang,[b] Mingyu Zhang,[b] Liwen Zhang,[b] Yufeng Xin,[bc] Yanyan Liu[b] and Junfeng Chen*[b]

Received 30th September 2024
Accepted 5th February 2025

DOI: 10.1039/d4ra07021f

rsc.li/rsc-advances

Zinc/cobalt metal–organic skeleton/carbon nanotubes (Zn/Co-ZIF@CNTs) were prepared by solvothermal method using Zn/Co-ZIF as the main raw material and CNTs as the carrier. The results showed that Zn/Co-ZIF@CNTs retained the high specific surface area and large porosity of ZIFs while exhibiting a stable cubic crystal structure. At the optimal initial dye concentration, the removal rates for methyl orange (MO) and methylene blue (MB) reached over 85%. When the dosage of Zn/Co-ZIF@CNTs was 30 mg in a 30 mL solution, the removal of MO and MB reached the maximum. The MO removal rate in mixed solution was generally lower than that in unmixed solution, and the removal rate of MB was the opposite. The second-order kinetic model was the most suitable for describing the adsorption of MO and MB by Zn/Co-ZIF@CNTs, and it was dominated by chemisorption. The reaction isotherms for the adsorption of MO were well fitted by the Langmuir model. The adsorption process for MB was consistent with the Freundlich adsorption isotherm model. The adsorption mechanism for MO and MB was mainly electrostatic interactions and π–π stacking; moreover, competitive adsorption and synergistic adsorption effects might be involved.

1. Introduction

The rapid development of the global economy and growing industrial demand have enabled the textile, leather, paper, printing, paint and other industries to achieve rapid development. Dyes, as important raw materials in these industries, have increased significantly in terms of demand and volume used. The production and use of dyes causes a large amount of dye wastewater discharge. This has become one of the main environmental pollution problems.[1,2] Most of the dyes with complex structures are toxic,[3,4] carcinogenic[5] and mutagenic.[6] Moreover, they are resistant to digestion, stable to light, heat and oxidants, and are refractory pollutants.[7,8] To achieve the desired color effect in the practical application of printing and dyeing technology, two or more dyes are usually chosen for combined dyeing. Therefore, finding effective methods to effectively remove dyes with complex components from wastewater is crucial. Dyes can be divided into anionic, cationic and non-ionic according to the charge characteristics when dissolved in water.[9] The studies to date have mainly focused on anionic and cationic dyes. Physical adsorption, coagulating sedimentation, ion exchange and photocatalytic oxidation are commonly used in the treatment of dye wastewater.[10] Among them, the adsorption method is widely used in the decolorization and degradation of dye wastewater due to its advantages of a wide range of adsorbents and materials, simple process, good decolorization effect and strong anti-pollution ability.[11] Methyl orange (MO), a typical anionic dye, is used in the printing and textile industry and is highly carcinogenic.[12] Methylene blue (MB) is a typical representative cationic dye. MB is used for dyeing silk, cotton and wood. MB occurs frequently in textile wastewater and is a serious hazard to humans and other organisms.[13]

The development and application of nanomaterials has driven advances in wastewater treatment technology, providing new solutions for dealing with complex and difficult to degrade pollutants. Manoj *et al.* reported that hydroxyapatite and hydroxyapatite/tantalum (HAp/Ta) core–shell nanostructured particles can be effectively used as a catalyst material for the treatment of industrial dye wastewater.[14] Alorku *et al.* reported that a nanomixture of 0-D ternary metal oxides (TiO_2–SnO_2–Al_2O_3) cooperating with 1-D hydroxyapatite (HAp) nanorods achieved 98% RhB degradation in acidic media with 20 ppm RhB in 90 min after UV irradiation. The adsorption method is widely used in dye wastewater treatment

[a]*Weifang University of Science and Technology, Shandong Peninsula Blue Economy and Engineering Research Institute, Shandong Engineering Research Center of Green and High-value Marine Fine Chemical, Weifang Key Laboratory of Chemical Wastewater Pollution Control and Resource Reuse, Weifang 262700, China*

[b]*School of Life Sciences, Qufu Normal University, Qufu 273165, P. R. China. E-mail: chenjunfeng@qfnu.edu.cn*

[c]*State Key Laboratory of Microbial Technology, Shandong University, Qingdao 266237, China*

† The two authors contributed equally.

due to its low cost, simple operation, green environmental protection, high selectivity and wide application range.[15] Currently, the commonly used adsorbents are activated carbon, bio-based, graphene, metal–organic framework (MOFs), *etc.* Among them, MOFs are coordination polymers with a three-dimensional stable structure formed by connecting metal ions or metal clusters with organic compounds through coordination bonds.[16] MOFs have the advantages of low mass density, high porosity, large specific surface area and controllable microporous structure in the field of adsorbing organic pollutants in water.[17,18] Zeolitic imidazolate frameworks (ZIFs) are a class of MOFs that are composed of imidazolate-bridged tetrahedral metal ions (such as Zn, Co). Compared with other MOFs, ZIFs feature the topological morphology of zeolites in structural and coordination factors, showing excellent permanent porosity, stability and adsorption capacity.[19] The properties, types and structures of ZIFs mainly depend on the different combinations of imidazole ligands and metal ions. The most representative ZIFs are ZIF-8 and ZIF-67 with rhombic dodecahedron structures synthesized by coordination of Zn^{2+} and Co^{2+} with dimethylimidazole ligands, respectively. They have high thermal and chemical stability and adjustable zero-type topology.[20] Nazir *et al.* prepared ZIF-67 nanocomposite doped with recycled metal Ni, which exhibited a good removal rate for methyl orange in water.[21] Nawz *et al.* reported a unique crystalline MoS_2@ZIF-67 nanocomposite adsorbent prepared using an *in situ* synthesis technique for the efficient removal of methyl MO dye from an aqueous medium.[22] Jiang *et al.* synthesized ZIF-8 *via* a hydrothermal method and found that its maximum adsorption capacity for Congo Red was 1 250 mg g^{-1}.[23] Mahmoud *et al.* prepared a polysulfone/ZIF-8 nanocomposite ultrafiltration membrane and achieved removal rates of up to 95.1% and 89.65% for methyl blue and crystal violet dyes.[24] Therefore, ZIFs have potential as adsorbents.

Carbon nanotubes (CNTs) are one-dimensional tubular nanomaterials with excellent physical properties, large specific surface area, easy functionalization and high mechanical strength; the tubes consist of multiple interconnected carbon atoms.[25,26] With the deepening of research, the application of carbon nanotubes is no longer limited to its inherent properties. Ma *et al.* successfully synthesized high specific surface area and mesoporous activated carbon nanotubes by an alkaline method, which exhibited excellent adsorption properties for anionic and cationic dyes in aqueous solution, especially methyl orange and methylene blue.[27] Single-walled CNTs showed a higher adsorption capacity (585 mg g^{-1}) for acid red B (ARB) than muti-walled CNTs.[28] ZIF-8 as a metal–organic skeleton was hybridized with CNTs and gave greater removal of malachite green than the MOF alone.[29] This demonstrated that adsorbents based on the combination of CNTs and ZIFs have good potential for the removal of dyes from aqueous solutions. CNTs and ZIFs adsorb dye molecules through their porous structure, thereby achieving the physical removal of these molecules. During the adsorption process, the noticeable fading of the dye solution's color served as a visual indication of the decolorization process. The extent of decolorization can be quantitatively analyzed by measuring the absorbance of the clear supernatant solution. The adsorption of dye molecules not only realizes their physical removal but is also accompanied by a decolorization effect.

Based on the above advantages, future research should focus on the combination of carbon nanotubes with other materials to synthesize new composite materials, thereby further improving the performance of the materials and achieving multifunctional applications. In recent years, in order to further explore materials with higher adsorption performance, excellent synergistic adsorption performance was achieved by mixing MOFs materials with other components to prepare composites to effectively adsorb dye pollutants in wastewater. Single-component dyes are often adsorbed using adsorbents, but the problem of adsorption of two-component dyes in wastewater is less studied. There is a lack of comprehensive understanding of the mechanism of adsorption of dye components by MOFs composites.

In this study, Zn/Co-ZIF bimetallic MOFs were prepared by solvothermal method and successfully compounded with CNTs to design Zn/Co-ZIF@CNTs. Zn/Co-ZIF@CNTs were used as an adsorbent to explore the effects of different factors on the adsorption performance under single-component and two-component dye systems. The interaction mechanism between Zn/Co-ZIF@CNTs and dyes was thoroughly investigated by combining some characterization methods and establishing a reaction kinetic model. The adsorbent material produced in this study can effectively adsorb the dye molecules and reduce the dye concentration in aqueous solution; it is not just a color change. The new material holds potential for treating dye wastewater with complex components.

2. Materials and methods

2.1 Chemicals

2-Methylimidazole, cobalt nitrate ($Co(NO_3)_2 \cdot 6H_2O$), zinc nitrate ($Zn(NO_3)_2 \cdot 6H_2O$), methyl alcohol (CH_3OH), multi-wall carbon nanotubes (MWCNT) (purity >95 wt%, with outer diameter of 8–15 nm and length of 3–12 μm, D50 ≤ 7 μm, specific surface area ≥250 m^2 g^{-1}), methyl orange, and methylene blue. All reagents and chemicals were of analytical grade and did not require further purification before use.

2.2 Synthesis of Co-ZIF

0.546 g of cobalt nitrate hexahydrate was dissolved in 15 mL of methanol to form a homogeneous solution. Separately, 0.616 g of 2-methylimidazole was also dissolved in an equal volume of methanol. After the cobalt nitrate solution was fully dissolved, it was mixed with the 2-methylimidazole methanol solution under ultrasonic assistance. The mixture was centrifuged twice at 11 000 rpm, and the resulting supernatant was redispersed in 15 mL of methanol. The cobalt nitrate methanol solution was then added to the separated solution, and the mixture was transferred to a Teflon-lined stainless steel autoclave. The autoclave was heated at 120 °C for 1 h. After the reaction, the solution was removed from the autoclave, and the reaction mixture was centrifuged again at 11 000 rpm. The washed

product was dispersed in a methanol solution for subsequent experimental analysis.

2.3 Synthesis of Zn-ZIF

0.71 g of zinc sulfate hexahydrate and 0.81 g of 2-methylimidazole were individually dissolved in 50 mL of methanol. The solutions were mixed and stirred for 5 min to ensure a homogeneous mixture. The combined solution was allowed to age at room temperature for 24 h, which resulted in a milky white suspension. Repeated centrifugation was performed at 9 500 rpm, followed by the addition of methanol and ultrasonic treatment for redispersion. Finally, the obtained white crystals were placed in a vacuum oven and dried overnight at 60 °C. The sample was then sealed in a sample vial for storage.

2.4 Synthesis of Zn/Co-ZIF@CNTs

At room temperature, 0.546 g of $Co(NO_3)_2 \cdot 6H_2O$, 0.558 g of $Zn(NO_3)_2 \cdot 6H_2O$, and 0.616 g of 2-methylimidazole were dissolved in 7.5 mL, 7.5 mL, and 15 mL of methanol, with ultrasonication for 5 min. The cobalt nitrate methanol solution was mixed with the 2-methylimidazole methanol solution under ultrasonic treatment for 10 min. Subsequently, the zinc nitrate methanol solution and a certain amount of CNTs were added to the mixed solution, which was again sonicated for 10 min. The resulting suspension was then transferred to a Teflon-lined stainless steel autoclave and heated at 120 °C for 4 h. Finally, fresh methanol was added, and the mixture was centrifuged at 11 000 rpm for 5 min. The Zn/Co-ZIF@CNTs product was obtained after repeated washing and drying with methanol (Fig. 1).

2.5 Characterization

Scanning electron microscopy (SEM, Phenom, China) was employed to meticulously examine the morphological features of the samples. Furthermore, Fourier transform infrared spectroscopy (FT-IR, NEXUS-670, USA) was employed to investigate the chemical bonds and functional group structures within the samples. The wave number range spanned from 400 cm^{-1} to 4000 cm^{-1}. Additionally, X-ray diffraction (XRD, Bruker D8 Advance, Germany) technology was utilized to determine the crystal structure of Zn/Co-ZIF@CNTs with the scanning parameters set at a rate of 2° per minute and a step size of 0.02°.

2.6 Adsorption experiments

The standard solutions of methyl orange and methylene blue were diluted to different concentration gradients. The concentration gradient of the standard curve for methyl orange was 2.5, 5, 7.5, 10, 12.5 and 15 mg L^{-1}. The concentration gradient of the standard curve for methylene blue was 1, 2, 3, 4, 5 and 6 mg L^{-1}. A UV-vis spectrophotometer was used to measure the absorbance of the solutions at their specific absorption wavelengths (the maximum absorption wavelength of methyl orange was 464 nm, and the maximum absorption wavelength of methylene blue was 664 nm), with distilled water as the reference solution. Based on the measurements, standard curve equations were established.

The experiment was conducted under natural light conditions. The composite material Zn/Co-ZIF@CNTs served as a decolorizing agent for the decolorization of dye solutions. Zn/Co-ZIF@CNTs could be separated from the effluent solution after the adsorption of dyes by simple means of centrifugation and filtration. The adsorption capacity, q, at time t, the saturated adsorption capacity (q_e), and the removal rate (R) of methyl orange and methylene blue dyes for the Zn/Co-ZIF@CNTs adsorbent were calculated according to the following equations:

$$q = \frac{(c_0 - c_t)V}{m} \quad (1)$$

$$q_e = \frac{(c_0 - c_e)V}{m} \quad (2)$$

$$R = \frac{c_0 - c_e}{c_0} \times 100\% \quad (3)$$

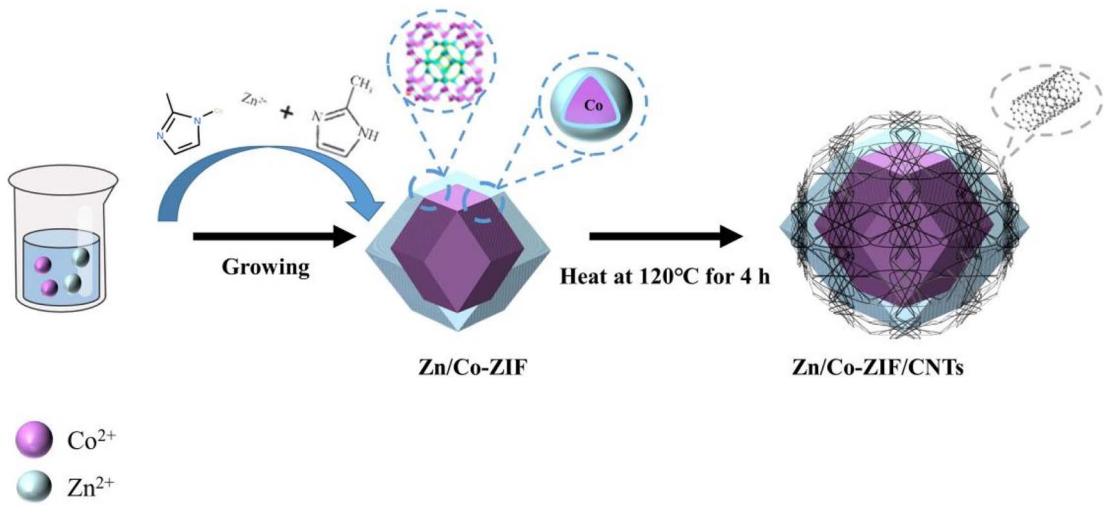

Fig. 1 The synthetic schematic diagram for preparing Zn/Co-ZIF@CNTs

In the equations: c_0 represents the initial mass concentration of the dye before adsorption, in mg L^{-1}; c_t represents the mass concentration of the dye at time t during adsorption, in mg L^{-1}; c_e represents the equilibrium mass concentration of the dye after adsorption, in mg L^{-1}; V represents the volume of the dye solution to be adsorbed, in L; and m represents the amount of adsorbent used, in g.

2.7 The fitting of the adsorption kinetics curve

The relationship between contact time and adsorption capacity in the process of Zn/Co-ZIF@CNTs adsorbing MO and MB was investigated in this study. Pseudo-first-order kinetic and pseudo-second-order kinetic models were employed to analyze and describe the kinetic process of dye adsorption.[30,31]

Pseudo-first-order kinetic model:

$$\ln (q_e - q_t) = \ln q_e - k_1 t \quad (4)$$

Pseudo-second-order kinetic model:

$$\frac{t}{q_t} = \frac{1}{k_2 q_e^2} + \frac{t}{q_e} \quad (5)$$

In the equations: q_e represents the equilibrium adsorption capacity, in mg g^{-1}; q_t represents the adsorption capacity at time t, in mg g^{-1}; t represents the adsorption time, in min; k_1 is the reaction rate constant of the pseudo-first-order kinetic equation, in min^{-1}; and k_2 is the reaction rate constant of the pseudo-second-order kinetic equation, in g $(mg\ min)^{-1}$.

2.8 The fitting of adsorption isotherm

To further investigate the adsorption behavior of Zn/Co-ZIF@CNTs towards MO and MB, the adsorption isotherm models, specifically the Langmuir adsorption isotherm model and the Freundlich adsorption isotherm model,[32,33] were established using the adsorption equilibrium data.

Langmuir adsorption isotherm model:

$$\frac{c_e}{q_e} = \frac{c_e}{q_m} + \frac{1}{q_m K_L} \quad (6)$$

Freundlich adsorption isotherm model:

$$\ln q_e = \ln K_F + \frac{1}{n} \ln c_e \quad (7)$$

In the equations: c_e represents the equilibrium concentration of the dye in the solution after adsorption by the adsorbent, in mg L^{-1}; q_e represents the equilibrium adsorption capacity of the adsorbent for the dye, in mg g^{-1}; q_m represents the maximum adsorption capacity of the adsorbent, in mg g^{-1}; K_L represents the Langmuir adsorption constant, in L mg^{-1}; K_F represents the Freundlich adsorption constant, in mg $(L\ mg)^{-1}$; $1/n$ represents the adsorption intensity, and a larger value of n indicates a more favorable adsorption process.

2.9 Investigation of the effect of the initial concentration of the solution on the removal rate

MO and MB solutions with different concentration gradients were prepared (400, 500, 600, 750, 1000, 1250, 1500 and 2000 mg L^{-1}). 0.015 g of Zn/Co-ZIF@CNTs was added to 30 mL of the solution. The absorption was carried out in a thermostatic oscillator at 150 rpm. Multiple samples were taken over a period of time (10 min, 20 min, 30 min, 40 min, 50 min, 1 h, 2 h, 3 h, 4 h). The samples underwent centrifugation at 8000 rpm for a duration of 10 min to facilitate the separation from the residual adsorbent. Subsequently, the residual concentrations of MO and MB were determined spectrophotometrically at wavelengths of 464 nm and 664 nm, respectively, employing a UV-vis spectrophotometer. Considering the adsorption properties of the material for the mixed dye solution, five representative sets of dye solutions were selected for mixing. The concentration ratio of the components in the dye mixtures was 1 : 1. The other operations were the same as above. The absorbance of the solution was measured at different wavelengths. The studies were performed at room temperature.

2.10 Investigation of the effect of adsorbent quality on removal rates

Under the initial conditions, the MO and MB solution concentrations were 2000 mg L^{-1} and 50 mg L^{-1}. The volume of the water sample was 30 mL. A mass gradient of adsorbent was established and added into the water sample (5, 10, 15, 20, 25, 30 and 35 mg), and they were adsorbed in a thermostatic oscillator at 150 rpm. Multiple samples were taken at intervals. The adsorption process was concluded within a period of 1 h. Subsequent to this, the samples were subjected to centrifugation at a speed of 8000 rpm for a duration of 10 min. The absorbance was measured by UV spectrophotometry and converted into concentration. The studies were performed at room temperature. Similarly, the influence of the amount of adsorbent applied on the adsorption performance for the two-component dye system was explored. Representative concentrations of MO and MB solutions were mixed to obtain a 30 mL water sample. The same adsorbent mass gradient as for the individual components was established. All other operations were the same as the above. The studies were performed at room temperature.

3. Results and discussion

3.1 Analysis of material morphology and structure characteristics

3.1.1 Morphological characteristics of Zn/Co-ZIF@CNTs. As depicted in Fig. 2, SEM characterization was conducted on Zn/Co-ZIF@CNTs, yielding clear images of the crystal morphology at various magnifications. In Fig. 2a, it was demonstrated that the synthesized Zn/Co-ZIF crystals maintain a well-defined dodecahedral structure, characterized by regular geometric shapes and stable crystal structures. Zinc and cobalt atoms serve as metal-centered nodes, engaging in coordination with imidazole ligands to assemble a Zn/Co-ZIF framework,

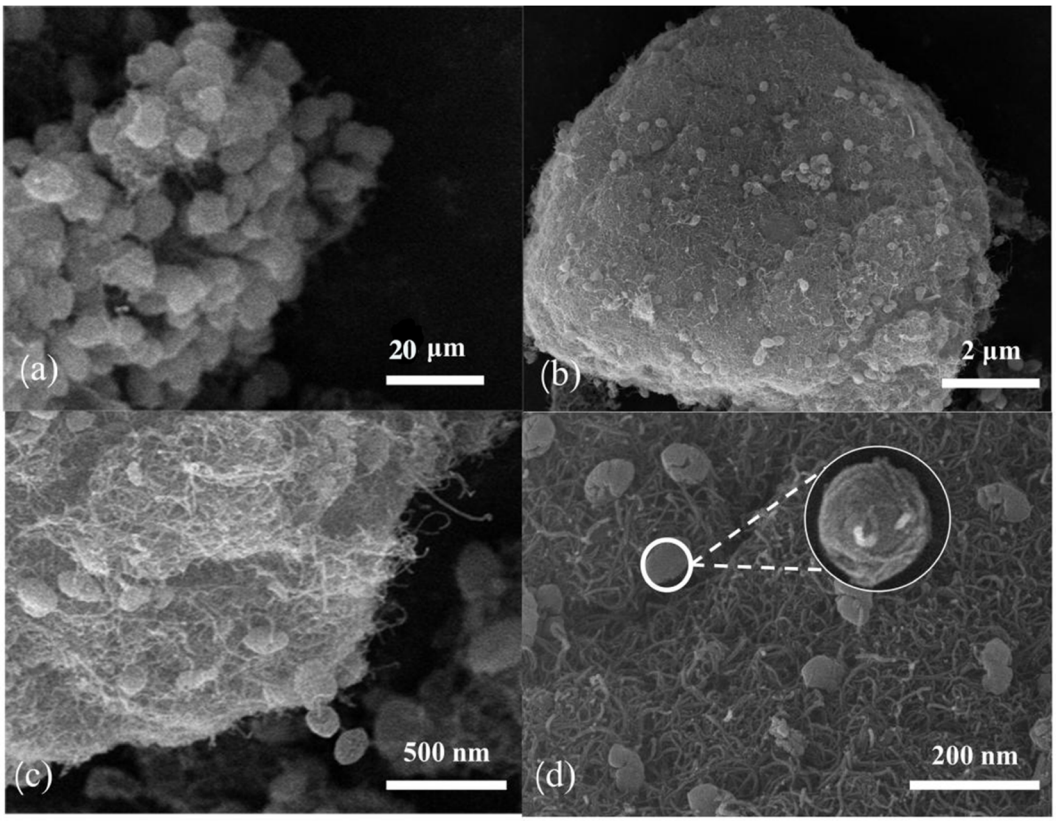

Fig. 2 The SEM of Zn/Co-ZIF@CNTs (a) 20 μm, (b) 2 μm, (c) 500 nm, (d) 200 nm.

which constitutes the active site. The imidazole layer supplied nitrogen atoms for metal ion coordination and was crucial for constructing the porous structure of the MOF. In Fig. 2b, the CNT clusters are uniformly adhered to the surface of the Zn/Co-ZIF crystal particles, which may contribute to enhancing the mechanical properties and stability of the material. With an increase in magnification in Fig. 2c and d, it can be observed that the surface of the synthesized Zn/Co-ZIF material is extensively wrapped by a multitude of linear structures, which were identified as carbon nanotubes. CNTs serve as physical supports in the MOF composites and were integrated into the MOF crystals to form interpenetrated structures. Fig. 2d reveals that the carbon nanotubes are tightly entwined around the surface of the Zn/Co-ZIF crystal particles, preliminarily confirming the successful fabrication of the Zn/Co-ZIF@CNTs. Relevant literature suggests that the unique morphological features of the surface might exert a certain influence on its performance.[34,35] The Zn/Co-ZIF@CNTs material has been optimized with respect to its structural and functional attributes through the integration of the metal–organic framework and carbon nanotubes.

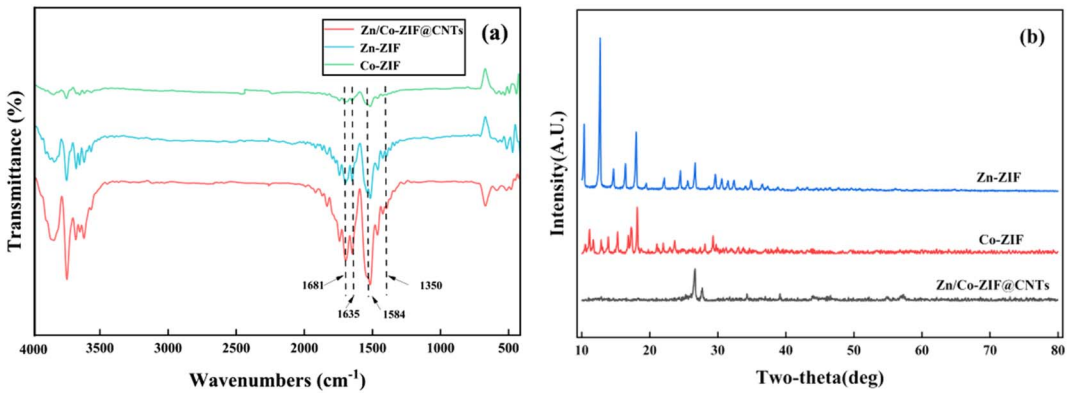

Fig. 3 (a) FT-IR spectra for Zn/Co-ZIF@CNTs and Co-ZIF and Zn-ZIF. (b) XRD patterns for Zn/Co-ZIF@CNTs and Co-ZIF and Zn-ZIF.

3.1.2 Structural characteristics of Zn/Co-ZIF@CNTs. Fig. 3a show the FT-IR spectra of Zn-ZIF, Co-ZIF and Zn/Co-ZIF@CNTs. The FT-IR spectra of all three materials show distinct absorption peaks at 1681 and 1584 cm^{-1}, indicating that all three contain N–H bonds, and the two peaks correspond to the tensile and bending vibration modes of the N–H bonds, respectively.[36] Meanwhile, the peaks at 1635 cm^{-1} and 1584 cm^{-1} indicate the stretching vibration of the C=N bond in addition to the bending vibration of the N–H bond.[37] The FT-IR spectra of three ZIFs in the range of 1350–1500 cm^{-1} show a series of strong spin bands that are related to the stretching of the imidazole ring and the bending vibration of its C–H bond.[38] The upward peaks of Co-ZIF and Zn-ZIF at 500–750 cm^{-1} contrast with the downward peaks of Zn/Co-ZIF@CNT, likely due to the CNTs altering the imidazole ring's chemical environment and modifying the infrared absorption properties, thus affecting the peak direction in FT-IR spectra.[39] The absorption peak observed at 422 cm^{-1} was attributed to the stretching vibrations of the Zn–N and Co–N bonds. The lack of discernible metal–oxygen bond absorption peaks suggests that the material exhibits metallic characteristics and was not present in its oxide form. The detection of characteristic Zn–N and Co–N peaks confirmed the successful coordination of metal ions with 2-methylimidazole. The nitrogen atom on the imidazole ring formed coordination bonds with cobalt and zinc metal ions, which is a key feature in MOF structures. In summary, the characteristic peaks of Zn-ZIF and Co-ZIF were successfully retained in the FT-IR spectra of the experimentally prepared Zn/Co-ZIF@CNTs. This result suggests the synthesis of a novel composite material by combining Zn-ZIF and Co-ZIF with CNTs. The prepared material not only inherited the chemical properties of the original ZIFs but also exhibits new physicochemical properties owing to the introduction of carbon nanotubes. The surface modification with CNTs was achieved by forming carboxyl and other functional groups, which improved their surface properties and thereby enhanced their interaction with ZIFs.

To deeply analyze the internal crystal structure characteristics of Zn/Co-ZIF@CNTs, XRD analysis was conducted on Zn/Co-ZIF@CNTs, Co-ZIF, and Zn-ZIF. In Fig. 3b, Co-ZIF and Zn-ZIF exhibit sharp diffraction peaks, and the relative positions and intensities of the diffraction peaks are consistent with the reported literature, indicating the successful synthesis of the materials with high purity and crystallinity.[40] Clear characteristic diffraction peaks of Zn/Co-ZIF@CNT appear near 2θ = 26.67° and 27.70°, respectively corresponding to the (134) and (044) crystal planes, which show the chaotic structure with low crystallinity.[41,42] This implies that the atomic arrangement of the material is less ordered than that of highly crystalline materials, resulting in a potentially heterogeneous structure. This was deduced from C=C stretching vibrations, and favored the adsorption of dye molecules.[43] The XRD pattern showed characteristic diffraction peaks of metal–organic frameworks, and hence the prepared material possesses metallic properties.

3.2 Analysis of influencing factors

3.2.1 The effect of different dye concentrations on removal rates. Fig. 4 illustrates the effects of the initial concentrations of MO and MB on the adsorption properties of Zn/Co-ZIF@CNTs (absorbent: 30 mg; solution: 60 mL). As the MO concentration increases from 800 mg L^{-1} to 3500 mg L^{-1}, the adsorption capacity constantly increases in Fig. 4a. The maximum adsorption capacity of 8425.65 mg g^{-1} was achieved with an initial MO concentration of 3500 mg L^{-1}. When the initial MO concentration was below 1500 mg L^{-1}, the removal rate increased with increasing concentration. The MO removal peaked at 94% at an initial concentration of 1500 mg L^{-1}, and then decreased with increasing concentration. Fig. 4b indicates that the adsorption capacity increased continuously when the initial MB concentration increased from 100 mg L^{-1} to 1300 mg L^{-1}. The maximum adsorption capacity reached at an initial MB concentration of 1300 mg L^{-1} is 203.91 mg g^{-1}. The removal rate of MB decreased with increasing initial concentration. The maximum removal rate of 86% was reached at a concentration of 100 mg L^{-1}. During the initial phase of MB adsorption, the removal rate decreased, potentially due to competition for available adsorption sites. As the dye concentrations increased, the adsorptive sites became progressively occupied, necessitating competition among newly added dye

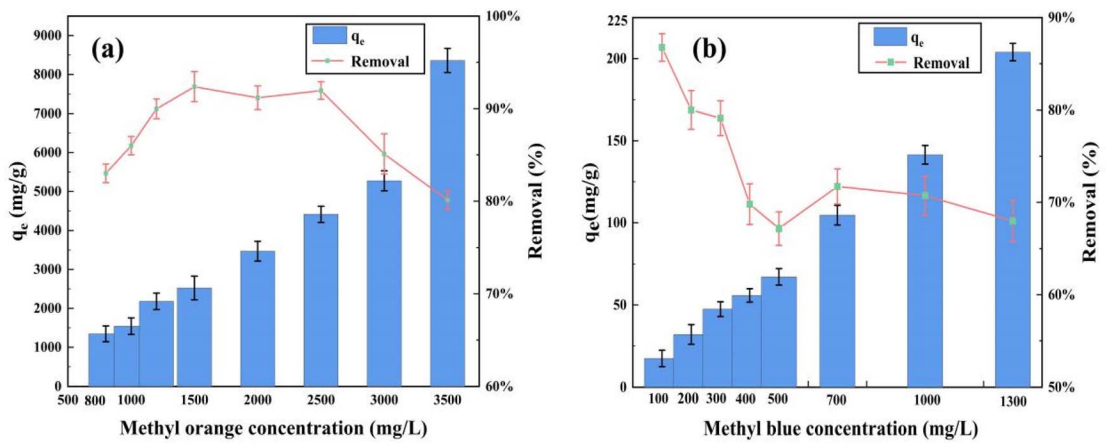

Fig. 4 Effects of the initial concentration of single-component dyes on the adsorption capacity of Zn/Co-ZIF@CNTs: (a) MO and (b) MB.

molecules and those already adsorbed for the remaining sites. By comparison, it was found that with the increase of the initial concentration, the removal rate of both dyes showed a downward trend. The adsorption capacity showed an increasing trend. This was mainly because a certain amount of adsorption sites on the adsorbent were limited and relatively stable. The disparity in the removal efficiencies of MO and MB by the adsorbents can be ascribed to the variations in their molecular interactions with the adsorbents, which are influenced by the distinct molecular structures and chemical properties of these dyes. When the dye reached a certain concentration, the adsorption sites of the adsorbent were saturated, and the adsorption capacity for the dye decreased.[44] Simultaneously, an increase in the initial dye concentration resulted in an increase in the amount of unadsorbed dye, leading to a decrease in removal efficiency. When the dye concentration was high, the opportunity for dye molecules to come into contact with the adsorbent surface increased. This fully utilized the adsorption sites of the adsorbent. Higher concentrations could promote electrostatic and non-electrostatic attraction between the dye and the adsorbent, thereby adsorbing more dye.[45] After multiple cycles, the adsorption performance of Zn/Co-ZIF@CNTs did not show a significant decrease, demonstrating its excellent recyclability and stability.

Fig. 5a–f shows the effect on the adsorption properties of Zn/Co-ZIF@CNTs under mixed dye fractions. The adsorption of MO by Zn/Co-ZIF@CNTs in the mixed solution is shown in Fig. 5a–c. Typical initial concentrations of mixed MO and MB (red line) were selected and compared to the removal rates of unmixed MO and MB (green line) at the same concentrations. The results show that the removal rate of MO in the mixed solution was generally lower than that in the unmixed solution. This might be due to the competition of MB with MO for the adsorption sites, which affects the MO adsorption efficiency. In addition, the data in Fig. 5d–f reveal the adsorption performance of Zn/Co-ZIF@CNTs for MB in mixed solutions. The results show that the MB removal rate in the mixed solution is generally higher than that in the unmixed MB solution. Therefore, Zn/Co-ZIF@CNTs showed better adsorption performance in treating mixed dye wastewater containing MB.

3.2.2 The effect of adsorbent mass on removal rates. The effects of different adsorbent masses on the adsorption of MO and MB under the single-component dye system are shown in Fig. 6. The results show that the removal of both MO and MB by Zn/Co-ZIF@CNTs increased with the increase of the adsorbent content. The increase in the adsorbent content provided more adsorption active sites and increased the contact area between the adsorbent and the dye, which is favorable for adsorption. When the adsorbent dosage was 30 mg, the removal of dyes reached the maximum in both cases. The maximum removal efficiency was 98% for MO and 83% for MB. However, when the adsorbent dosage was more than 30 mg, the removal of dyes was almost unchanged. This was because the adsorption system reached adsorption equilibrium. The increased adsorption sites were in an unsaturated state. It was observed that the adsorption capacity of both MO and MB showed a decreasing trend with the increase of the adsorbent content. This was due to the fact that too much adsorbent caused the effective adsorption sites on the surface to overlap. Fewer effective adsorption sites were available per unit mass of adsorbent.[46] This led to a longer diffusion path for MO and MB to reach the adsorbent surface and decreased adsorption capacity.

In Fig. 7a and b, the MO and MB removal efficiency reached the maximum value when the adsorbent dosage of 30 mg was

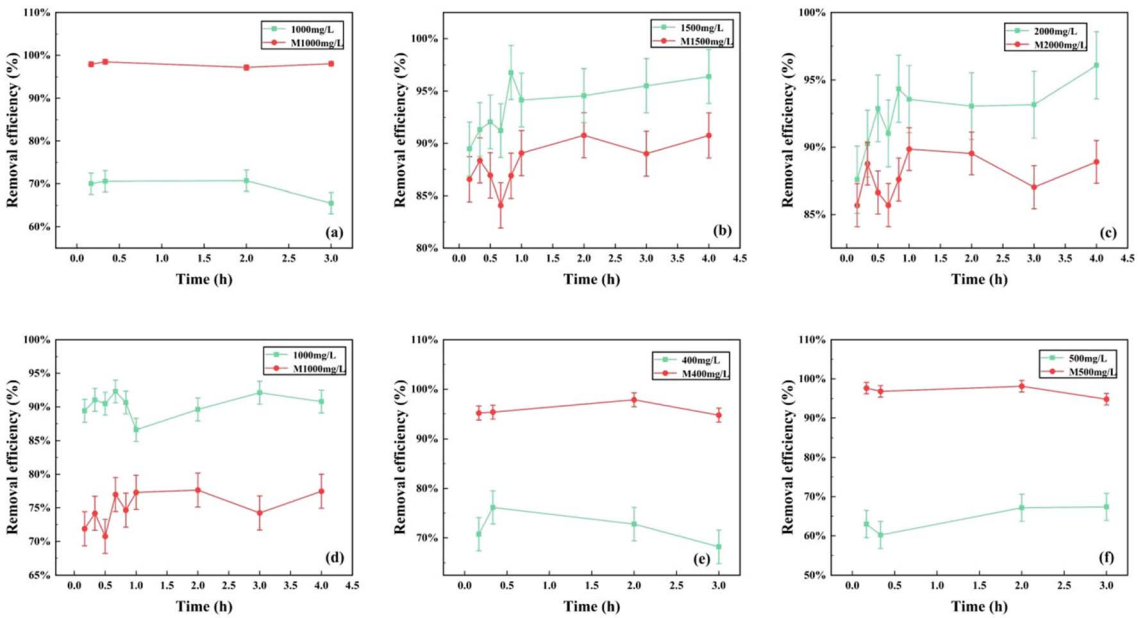

Fig. 5 Removal rate of Zn/Co-ZIF@CNTs for different mixed concentrations of MO and MB: (a) MO 1000 mg L^{-1}, (b) MO 1500 mg L^{-1}, (c) MO 2000 mg L^{-1}, (d) MB 400 mg L^{-1}, (e) MB 500 mg L^{-1}, and (f) MB 1000 mg L^{-1}.

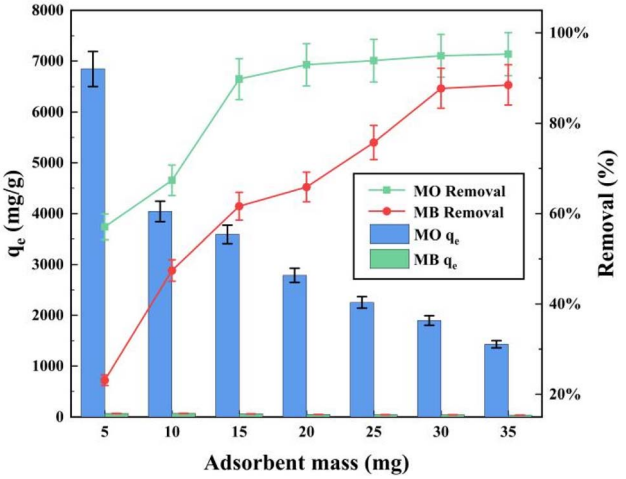

Fig. 6 Effect on the adsorption capacity of Zn/Co-ZIF@CNTs for a single component dye: MO and MB.

added to the solution for both mixed and unmixed dye solutions. The removal of dyes remained almost constant after adsorbent addition of more than 30 mg. The removal efficiency of MO changed from 98% to 91% and the removal efficiency of MB increased from 83% to 88%. This result was similar to the change in the removal efficiency observed before and after dye mixing in Fig. 5. In summary, the effect of adsorbent addition for the mixed dye solution on the adsorption performance of Zn/Co-ZIF@CNTs was similar to that for the unmixed solution. The maximum adsorption effect was reached at an adsorbent dose of 30 mg. The amount of adsorbent added changed the removal efficiency of MO and MB both before and after dye mixing. Both results showed better adsorption performance of Zn/Co-ZIF@CNTs for treating MB in mixed dye wastewater.

3.3 Adsorption kinetics

The adsorption process consists of three stages: initially, the solute molecules come into contact with and are integrated onto the surface of the adsorbent. Subsequently, the solute molecules diffuse into the pores of the Zn/Co-ZIF@CNTs. Finally, solute molecules are bound at specific adsorption sites of the adsorbent to complete the adsorption process.[47] To further investigate the mass transfer, diffusion, and adsorption processes in dye removal, the experimental data were fitted to the pseudo-first-order kinetic and pseudo-second-order kinetic models using eqn (4) and (5). The results are presented in Fig. 8 and Table 1.

In Table 1, the pseudo-first-order kinetic model coefficient R^2 for the adsorption of MO onto Zn/Co-ZIF@CNTs was 0.405. The pseudo-second-order kinetic model coefficient R^2 was 0.999. For the adsorption of MB onto Zn/Co ZIF/CNTs, the pseudo-first-order kinetic model coefficient R^2 was 0.973. The pseudo-second-order kinetic model coefficient R^2 was 0.998. Additionally, the calculated equilibrium adsorption capacities from the pseudo-second-order kinetic models for MO and MB were close to the actual values. These data indicate that the adsorption processes of MO and MB onto Zn/Co-ZIF@CNTs follow the pseudo-second-order kinetic model more closely, which suggests that the interaction between the material and the dyes is the rate-controlling step. The results show that this is a chemical adsorption process.[48]

3.4 Adsorption isotherms

The data for the adsorption of MO and MB by Zn/Co-ZIF@CNTs were fitted according to the Langmuir and Freundlich adsorption isotherm models. The isotherms were plotted as shown in Fig. 9, and the corresponding parameters are listed in Table 2. As shown in Table 2, the R^2 in the Langmuir isothermal adsorption model for the adsorption process of Zn/Co-ZIF@CNTs on MO was more than 0.99, and higher than the R^2 for the Freundlich adsorption isotherm model. The adsorption of MO by Zn/Co-ZIF@CNTs was more consistent with the Langmuir isothermal model, primarily exhibiting monolayer adsorption characteristics.[49] According to the Langmuir adsorption isotherm fitting, the adsorption of MO and MB exhibited values of $0 < K_L < 1$, suggesting a relatively facile adsorption process. From the Freundlich adsorption isotherm fitting data, it was observed that the R^2 for MB was closer to 1.

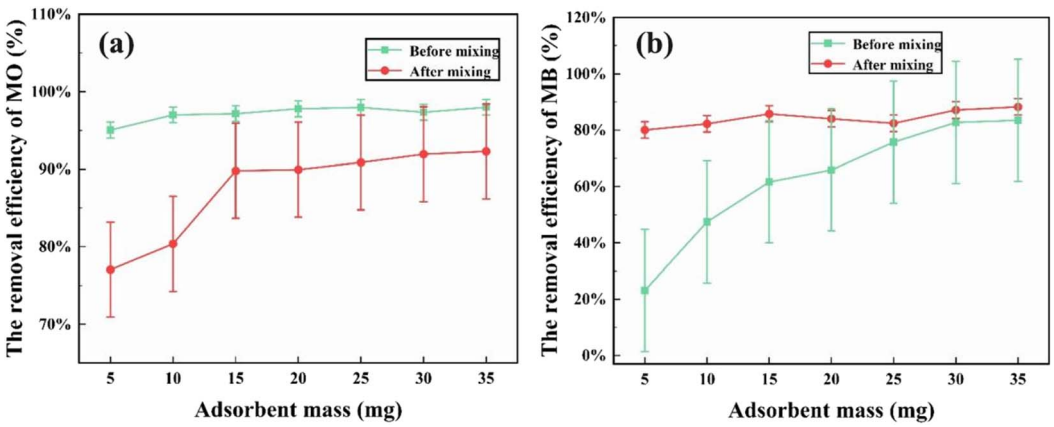

Fig. 7 Removal rate of Zn/Co-ZIF@CNTs for different sorbent content: (a) MO and (b) MB.

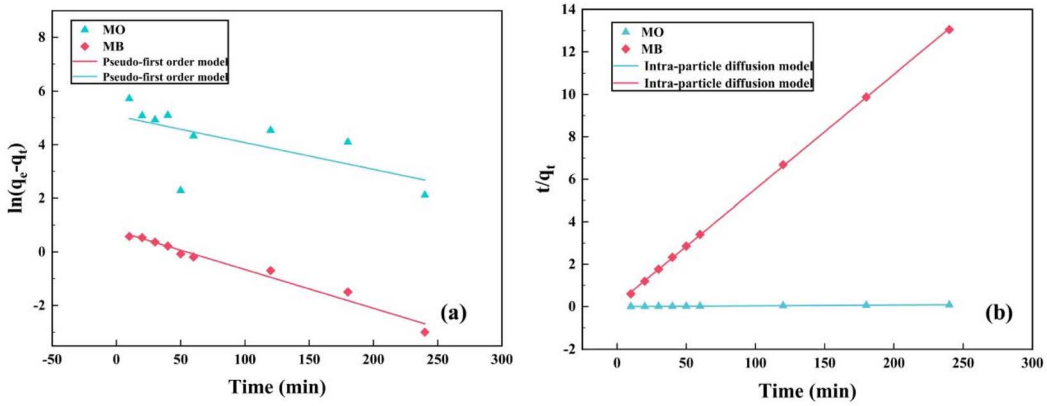

Fig. 8 The adsorption kinetics of MO and MB: (a) pseudo-first order kinetic and (b) pseudo-second-order kinetic.

Table 1 Pseudo-first order and pseudo-second-order kinetic parameters of Zn/Co-ZIF@CNTs for different initial dye concentrations

	Pseudo-first-order			Pseudo-second-order			Experimental value
Samples	K_1 (10^3 min^{-1})	q_e (mg g^{-1})	R^2	K_2 (10^3 min^{-1})	q_e (mg g^{-1})	R^2	q (mg g^{-1})
MO	23.03	154.56	0.405	0.24	3333.33	0.999	2901
MB	33.39	2.20	0.973	21.21	18.52	0.998	18.45

Therefore, the adsorption process of MB onto Zn/Co ZIF/CNTs follows the Freundlich adsorption isotherm model, with multilayer physical adsorption as the primary mechanism.[50] Additionally, for both dyes, the $1/n$ values were within the range of 0–1. For MO adsorption, $K_F = 843.872 > 2.687$, indicating that the adsorption process of Zn/Co-ZIF@CNTs for dyes was relatively facile. The adsorption capacity for MO was more than that for MB. Zn/Co-ZIF@CNTs have certain advantages as a dye adsorbent.

3.5 Dye removal comparison

Table 3 presents the rates of removal of MB and MO by various adsorbents. The dye removal by Zn/Co-ZIF@CNTs was very promising when compared with various adsorbents used to remove MO and MB from wastewater solutions, as shown in Table 3. The high adsorption capacity of Zn/Co-ZIF@CNTs and its comparison with the aforementioned materials suggested that the method of preparing composites using Zn-ZIF, Co-ZIF, and CNTs could provide superior dye removal.

3.6 Study of adsorption mechanism

ZIF-67 and ZIF-8 were identified as a class of novel porous materials with zeolite-like three-dimensional topological structures, abundant carbon–nitrogen ligands, and high metal ion content. Among various nanostructures, the nanotube structure is characterized by clear internal channels and a large specific

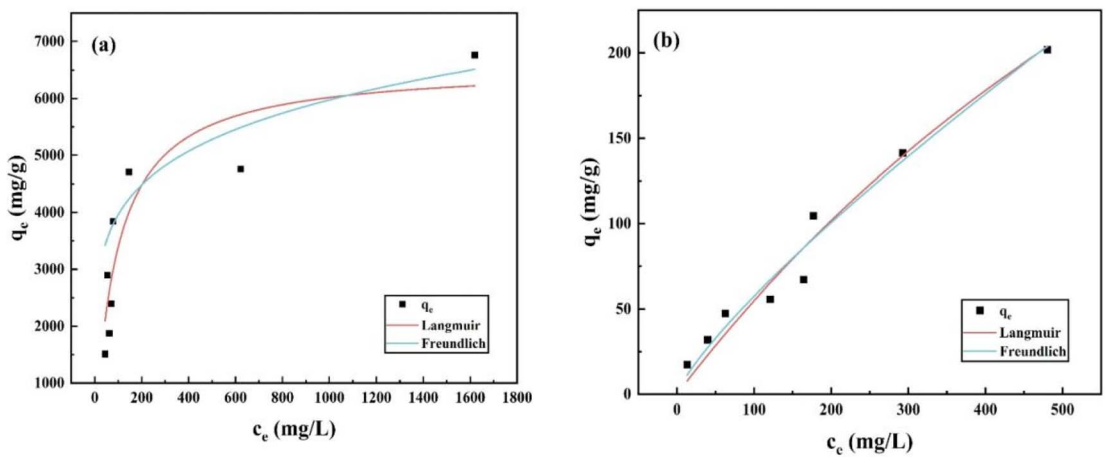

Fig. 9 Adsorption of (a) MO and (b) MB by Zn/Co-ZIF@CNTs. The Langmuir and Freundlich adsorption isotherm models were compared.

Table 2 Adsorption isothermal parameters for MO and MB on Zn/Co-ZIF@CNTs

	Langmuir			Freundlich		
Samples	K_L (L mg^{-1})	q_m (mg g^{-1})	R^2	K_F (g mg^{-1} min^{-1})	$1/n$ (mg g^{-1})	R^2
MO	0.0172	5000	0.995	843.872	0.2612	0.556
MB	0.0022	357.143	0.519	2.687	0.6809	0.961

Table 3 Comparison of dye removal capacity of different adsorbents

Adsorbent	Preparation method	Dye	Concentration (mg L^{-1})	Reaction time (min)	Removal rate (%)	Reference
MOF-525(Co)	Metalation	MO	100	60	90.5	51
CS/MOF-235	Solvo-thermal	MO	1500	20	87	52
Mn@ZIF-8	Hydrothermal	MO	50	300	91.71	53
MOF-199	Solvo-hydrothermal	MB	4.5	16	80	54
SnO_2	Co-precipitation	MB	25	60	60	55
Cu-MOF	Ultrasonication	MB	70	720	50.71	56
Zn/Co-ZIF@CNTs	Hydrothermal	MO	2000	120	93.16	This study
Zn/Co-ZIF@CNTs	Hydrothermal	MB	1500	120	81.42	This study

surface area. Through the determination of the experimentally obtained XRD patterns matching the standard patterns of ZIF-67 and ZIF-8, the structure of Zn/Co-ZIF@CNT was confirmed to possess the characteristics of both ZIF-67 and ZIF-8. SEM was employed to observe the specific morphologies of the synthesized material, thereby ascertaining the presence of ZIF-67 and ZIF-8 structures within the Zn/Co-ZIF@CNT composite. Under illumination conditions, the material may be excited to generate electron–hole pairs.[57] The high removal efficiency of MO and MB by Zn/Co-ZIF@CNTs was attributed to the synergistic effect of the two metals, which formed a three-dimensional structure with a high surface area and large pore capacity. The incorporation of CNTs endowed the material with a higher surface area and more adsorption sites.[58] This rendered the synthesized composite with a pronounced adsorption tendency. During the adsorption process, the dye molecules may interact with the active sites of

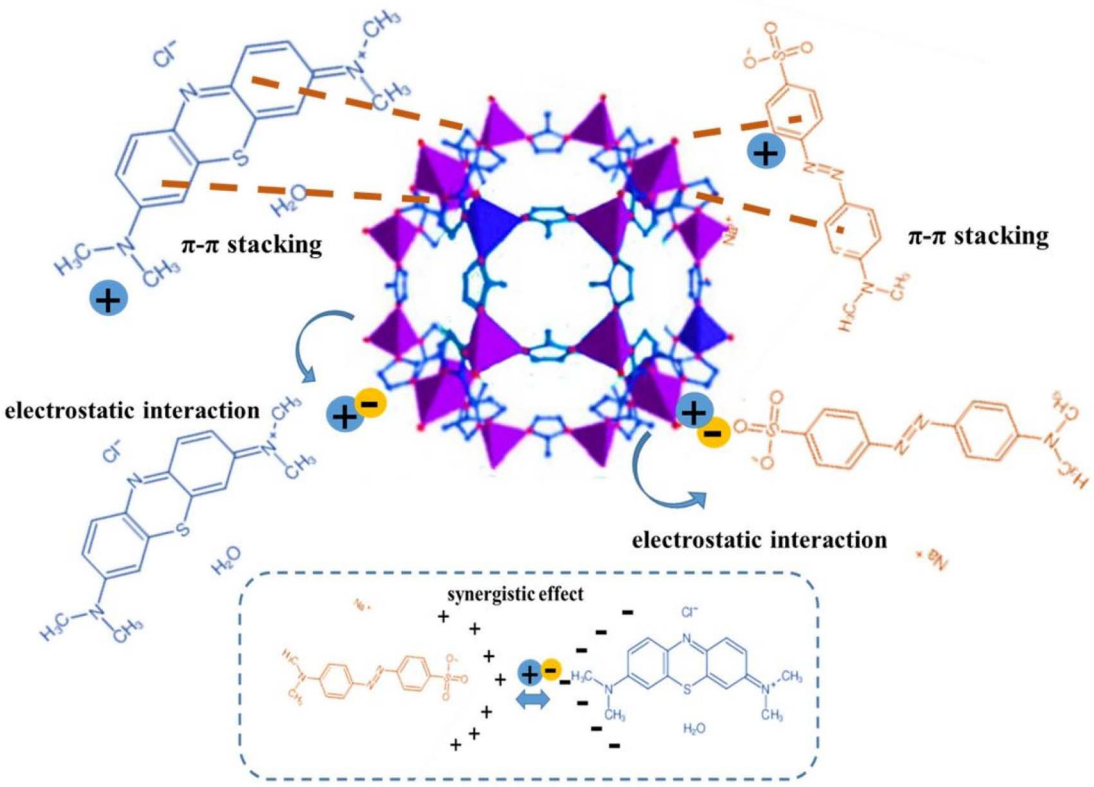

Fig. 10 The possible adsorption mechanism of Zn/Co-ZIF@CNTs for MO and MB.

the Zn/Co-ZIF@CNTs. The adsorption efficacy of the adsorbent was also related to the type of dye. Experiments indicated that the removal efficiency of MO was more than that of MB. MO, as a typical anionic adsorbate, and MB, as a typical cationic adsorbate, are distinguished by their charge characteristics. The charge distribution in the materials was determined by the coordination interactions between metal ions and organic ligands. In these structures, metal ions carried a positive charge, while organic ligands bore a negative charge. Under non-illuminated conditions, Zn/Co-ZIF@CNTs primarily rely on physical and chemical adsorption mechanisms for the removal of dyes. MO was attracted to the positively charged ZIF-67 under experimental conditions due to electrostatic interactions. Conversely, MB was repelled by ZIF-67 under the same conditions.[59] MB has a small molecular size to diffuse into the interior of Zn/Co-ZIF@CNTs and exhibited a strong adsorption capacity. In the Zn/Co-ZIF@CNTs material, hydrogen bonding is possible, especially in the layered structure, where hydrogen bonds act as a connecting force. π–π stacking is also a reason for dye adsorption. Both MO and MB dye molecules contain aromatic components, such as benzene rings, which allow π–π stacking with the imidazole ring in the adsorbent to promote adsorption. Although the aromatic ring structures of MO and MB theoretically formed π–π stacking with the imidazole rings in the ZIF-67 framework, the experimental results showed that the adsorption effect of ZIF-67 on MB was not ideal. This suggested that electrostatic interactions between opposite charges were the decisive dominant factors in the adsorption process.

In the binary dye system, competitive adsorption and synergistic adsorption effects were observed.[60] Owing to competitive adsorption, the removal rate of MO in the mixture of dyes was lower than the removal rate of single-component MO. The removal rate of MB in the mixture of dyes increased. Under the mixed system, MB was more likely to interact with the adsorption active sites of Zn/Co-ZIF@CNTs than MO. The coexisting MO molecules increased the removal efficiency of MB. MO molecules were adsorbed by various mechanisms, such as electrostatic attraction and π–π stacking, which promoted the movement of MB toward the adsorbent to complete the adsorption.[61] A synergistic adsorption process between MO and MB was achieved (Fig. 10).

4. Conclusions

In this study, Zn/Co-ZIF@CNTs were prepared by solvothermal method. Zn/Co-ZIF@CNTs maintained a robust stereostructure, which retained the advantages of large specific surface area and high porosity of ZIFs and CNTs. Zn/Co-ZIF@CNTs showed strong adsorption capacity for MO and MB. Zn/Co-ZIF@CNTs showed optimal adsorption with initial MO and MB concentrations of 1500 mg L^{-1} and 100 mg L^{-1}, respectively. Zn/Co-ZIF@CNTs showed the highest removal efficiency for MO and MB with a 30 mg dose of adsorbent in 30 mL of solution. In the mixed dye system, Zn/Co-ZIF@CNTs showed better MB adsorption than the dye alone, with the opposite result for the MO. The kinetics of Zn/Co-ZIF@CNTs for MO and MB were consistent with the pseudo-second-order model. The reaction isotherms of MO were well fitted by the Langmuir model. The adsorption process of MB conformed to the Freundlich adsorption isotherm model, which was dominated by multilayer adsorption. The adsorption mechanism of MO and MB mainly depended on electrostatic interactions and π–π interactions. Competitive and synergistic adsorption effects may exist in mixed dye systems.

Data availability

All relevant data are within the paper.

Conflicts of interest

The authors declare that they have no known competing financial interests or personal relationships that could have appeared to influence the work reported in this paper.

Acknowledgements

The authors were very grateful for the financial support provided by Shandong Postdoctoral Science Foundation (SDCX-ZG-202400174), Weifang University of Science and Technology Fund (2022KJ06, 2024XJKJ02), the Project of Weifang Science and Technology Development Plan (2024JZ0009), State Key Laboratory of Microbial Technology Open Projects Fund (Project No. M2023-06), the Innovation Capacity Enhancement Project of Science and Technology-based Small and Medium-sized Enterprises (2023TS1005, 2023TSGC0736) and Shandong Provincial Natural Science Foundation (ZR2024ZD39).

References

1 M. A. M. Nor, K. K. Ong, S. Mohamad, N. A. A. Nasaruddin, N. L. A. Jamari and W. M. Z. W. Yunus, *Mater. Res. Innovations*, 2014, **18**, 6.
2 H. Hou, R. Zhou, W. Peng and W. Lan, *Chem. Eng. J.*, 2012, 211–212.
3 M. S. Tsuboy, J. P. F. Angeli, M. S. Mantovani, S. Knasmüller, G. A. Umbuzeiro and L. R. Ribeiro, *Toxicol. In Vitro*, 2007, **21**, 8.
4 M. P. Shah, *Int. J. Environ. Biorem. Biodegrad.*, 2014, **2**, 1.
5 K. Golka, S. Kopps and Z. W. Myslak, *Toxicol. Lett.*, 2004, **151**, 1.
6 K. T. Chung, *J. Environ. Sci. Health, Part C*, 2000, **18**, 1.
7 Z. Aksu, *Biochem. Eng. J.*, 2001, **7**, 1.
8 K. Mahmoudi, K. Hosni, N. Hamdi and E. Srasra, *Korean J. Chem. Eng.*, 2015, **32**, 2.
9 M. T. Yagub, T. K. Sen, S. Afroze and H. M. Ang, *Adv. Colloid Interface Sci.*, 2014, **209**, 172–184.
10 T. A. Khan, M. Nouman, D. Dua, S. A. Khan and S. S. Alharthi, *J. Saudi Chem. Soc.*, 2022, **26**, 2.
11 Z. Zhang, H. Chen, W. Wu, W. Pang and G. Yan, *Bioresour. Technol.*, 2019, **293**, 122100.
12 A. Malathi, P. Arunachalam, J. Madhavan, A. M. Al-Mayouf and M. A. Ghanem, *Colloids Surf., A*, 2018, **537**, 435–445.
13 A. S. ALzaydien, *Am. J. Appl. Sci.*, 2009, **6**, 6.

14 M. Manoj, D. Mangalaraj, P. Meena and A. Yuan, *Mater. Res. Express*, 2020, **7**, 1.
15 K. Alorku, M. Manoj, C. Yanjuan, H. Zhou and A. Yuan, *Chemosphere*, 2021, **273**, 128575.
16 X. Li, W. Guo, Z. Liu, R. Wang and H. Liu, *Appl. Surf. Sci.*, 2016, **369**, 130–136.
17 N. A. Khan, Z. Hasan and S. H. Jhung, *J. Hazard. Mater.*, 2013, 244–245.
18 X. Fan, W. Wang, W. Li, J. Zhou, B. Wang, J. Zheng and X. Li, *ACS Appl. Mater. Interfaces*, 2014, **6**, 17.
19 F. Wang, Y. X. Tan, Y. Hui, H. X. Zhang, K. Yao and Z. Jian, *Chem. Commun.*, 2011, **47**, 20.
20 Y. Q. Tian, Y. M. Zhao, Z. X. Chen, G. N. Zhang, L. H. Weng and D. Y. Zhao, *Chem.-Eur. J.*, 2007, **13**, 15.
21 M. A. Nazir, T. Najam, K. Zarin, K. Shahzad, M. S. Javed, M. Jamshaid, M. A. Bashir, S. S. A. Shah and A. U. Rehman, *Int. J. Environ. Anal. Chem.*, 2021, **103**, 16.
22 T. H. Nawz, M. T. Masood, A. Safdar, M. Shahid, T. Noor, M. Hussain, A. Razi and M. A. Umer, *Micromachines*, 2023, **14**, 8.
23 C. L. Jiang, B. M. Fu, H. Cai and T. M. Cai, *Chem. Speciation Bioavailability*, 2016, **28**, 1–4.
24 M. E. Mahmoud, G. M. Nabil, M. A. Khalifa, N. M. El-Mallah and H. M. Hassouba, *Biointerface Res. Appl. Chem.*, 2019, **7**, 2.
25 J. T. Yoo, S. H. Lee, K. L. Chang, C. R. Kim, T. Fujigaya, H. J. Park, N. Nakashima and K. S. Jin, *RSC Adv.*, 2014, **4**, 91.
26 C. Wang, W. D. Xing, Y. L. Wu, Y. H. Li, Y. S. Yan, J. W. Zhu and Y. S. Yan, *Surf. Interfaces*, 2022, **31**, 101986.
27 J. Ma, F. Yu, L. Zhou, L. Jin, M. Yang, J. Luan, Y. Tang, H. Fan, Z. Yuan and J. Chen, *ACS Appl. Mater. Interfaces*, 2012, **4**, 11.
28 J. Jia, X. Peng, Z. Luan, B. Fan, J. Wang and C. Zhao, *Fresenius Environ. Bull.*, 2009, **18**, 5.
29 J. Abdi, M. Vossoughi, N. M. Mahmoodi and I. Alemzadeh, *Chem. Eng. J.*, 2017, **326**, 1145–1158.
30 T. Lu, J. Wang, C. Ye, Q. Zeng and L. Si, *Water Purif. Technol.*, 2015, **34**, 2.
31 G. Peng, D. Ding, N. Hu, Y. Yang and X. Wang, *CIESC J.*, 2011, **62**, 11.
32 H. Niu, Y. Zhang, Y. Liu, H. T. Niu, Y. Zhang, Y. Liu, N. Xin and W. D. Shi, *J. Colloid Interface Sci.*, 2019, **539**, 545–552.
33 A. S. Nateri, H. F. Juybari and A. Hivechi, *Indian J. Fibre Text. Res.*, 2019, **44**, 1.
34 T. T. T. Nguyen, H. T. Nguyen, H. T. Trinh, T. T. T. Bui, A. T. Le and T. Q. Huy, *Macromol. Res.*, 2022, **30**, 2.
35 K. Shiori and K. Katsunori, *Langmuir*, 2007, **23**, 23.
36 Z. Wang, B. Zhang, C. Ye and L. Chen, *Hydrometallurgy*, 2018, **180**, 262–270.
37 A. Yadav, P. Yadav, P. K. Labhasetwar and V. K. Shahi, *J. Environ. Chem. Eng.*, 2021, **9**, 6.
38 X. J. Guo, H. C. Yang, Q. Liu, J. Y. Liu, R. R. Chen, H. S. Zhang, J. Yu, M. L. Zhang, R. M. Li and J. Wang, *Chem. Eng. J.*, 2020, **382**, 122850.
39 C. Baudot, M. C. Tan and C. J. Kong, *Infrared Phys. Technol.*, 2010, **53**, 434–438.
40 X. Z. Kang, Z. W. Song and Q. Shi, *Asian J. Chem.*, 2013, **25**, 15.
41 W. Z. Xu, H. Y. Yan, G. S. Wang, Z. Q. Qin, L. J. Fan and Y. X. Yang, *Mater. Chem. Phys.*, 2021, **258**, 123810.
42 D. Tuncel and A. N. Oket, *Catal. Today*, 2021, **361**, 191–197.
43 W. Zhang, Y. Zhao, Q. Liao, Z. Li, D. Jue and J. Tang, *Molecules*, 2023, **28**, 2.
44 K. Gupta and O. P. Khatri, *J. Colloid Interface Sci.*, 2017, **501**, 11–21.
45 D. Özer, G. Dursun and A. Özer, *J. Hazard. Mater.*, 2007, **144**, 1–2.
46 W. Z. Tian, G. C. Ren, H. Cui, Y. Huan, P. Liu, L. P. Yang, Q. Jiang and X. Bai, *Int. J. Hydrogen Energy*, 2023, **48**, 38.
47 J. Ren, Z. Zhu, Y. Qiu, F. Yu, J. Ma and J. Zhao, *J. Hazard. Mater.*, 2020, **408**, 124846.
48 W. Cui, X. L. Kang, X. Y. Zhang and X. D. Cui, *J. Phys. Chem. Solids*, 2019, **134**, 165–175.
49 E. Salama, M. Ghanim, H. S. Hassan, W. A. Amer, E. Z. M. Ebeid, A. H. El-Shazly, M. Ossman and M. F. Elkady, *RSC Adv.*, 2022, **12**, 29.
50 S. Chen, L. M. Qiao, X. J. Feng, Y. F. Huang, G. L. Gao, J. Guan and D. H. Lin, *Pol. J. Chem. Technol.*, 2023, **25**, 1.
51 H. Lu, Q. Yang and B. Huang, *Microporous Mesoporous Mater.*, 2023, **360**, 112665.
52 T. Saeed, A. Naeem, I. U. Din, M. Farooq, I. W. Khan, M. Hamayun and T. Malik, *J. Hazard. Mater.*, 2022, **427**, 127902.
53 M. A. Nazir, M. A. Nazir, M. F. Elsadek, S. Ullah, I. Hossain, T. Najam, S. Ullah, N. Muhammad, S. S. A. Shah and A. U. Rehman, *Inorg. Chem. Commun.*, 2024, **165**, 112294.
54 A. H. Shah, C. Yuan, W. Y. Hao, W. H. Gu, S. Y. Liang, Z. Ul Abideen, F. Wahid and F. Teng, *J. Solid State Chem.*, 2022, **307**, 122835.
55 Z. Nasir, M. Shakir, R. Wahab, M. Shoeb, P. Alam, R. H. Khan, M. Mobin and G. Lutfullah, *Int. J. Biol. Macromol.*, 2017, **94**, 554–565.
56 M. D. Firouzjaei, F. A. Afkhami, M. R. Esfahani, C. H. Turner and S. Nejati, *J. Water Process Eng.*, 2020, **34**, 101180.
57 T. Sarker, I. Tahmid, R. K. Sarker, S. C. Dey, M. T. Islam and M. Sarker, *Polyhedron*, 2024, **260**, 117069.
58 T. Noor, U. Raffi, N. Iqbal, L. Yaqoob and N. Zaman, *Mater. Res. Express*, 2019, **6**, 12.
59 R. Ediati, P. Elfianuar, E. Santoso, D. O. Sulistiono and M. Nadjib, *Mesoporous Mater.*, 2019.
60 Y. Li, B. Pan, H. Y. Miao, H. M. Xu, X. F. Liu and G. Shi, *Chem. Res. Chin. Univ.*, 2020, **36**, 6.
61 B. Chen, F. X. Long, S. J. Chen, Y. R. Cao and X. J. Pan, *Chem. Eng. J.*, 2020, **385**, 123926.